ESHG

www.nature.com/ejhg

ARTICLE OPEN

Expanding the genetic landscape of Dusty Core Disease: new *RYR1* variants in Italian patients

Simona Zanotti[1], Francesca Magri[1], Sabrina Salani[2], Laura Napoli[3], Michela Ripolone[1], Serena Pagliarani[2], Dario Ronchi[2,3], Francesco Fortunato[3], Patrizia Ciscato[1], Denise Cassandrini[4,5], Fabiana Fattori[6], Maria Grazia D'Angelo[7], Emilio Albamonte[8], Vincenzo Nigro[9], Monica Sciacco[1], Stefania Corti[1,3], Giacomo Pietro Comi[2,3] and Daniela Piga[2]✉

Core myopathies are congenital diseases with clinical, pathological and genetic heterogeneity. Main histological features are fiber "cores" showing a focally reduced oxidative enzyme activity. Dusty Core Disease (DuCD) differs from Central Core Myopathy for the presence of irregular areas, without clear borders and round/ovoidal shape, and myofibrillar disorganization characterized by reddish purple granular material depositions. This disorder is defined clinically by severe phenotypes with early onset of disease and molecularly by low level of RyR1 in muscle. Until now DuCD was associated only to biallelic recessive *RYR1* mutations. We analyzed the clinical aspects, pathological features and mutational spectrum of four DuCD patients, belonging to our cohort of Congenital Myopathy probands. Molecular analysis detected 5 different *RYR1* pathogenic variants, two of them so far unreported. Patients presented a heterogeneous phenotype ranging from severe recessive infantile forms to moderate dominant adult-onset presentations. Histological, immunological and ultrastructural techniques were employed to validate these dominant cases, which expand our knowledge on the inheritance of this subgroup of diseases.

European Journal of Human Genetics; https://doi.org/10.1038/s41431-026-02080-3

INTRODUCTION

Core myopathies are congenital muscle diseases characterized by clinical and genetic heterogeneity. The main pathological feature at muscle biopsy is the presence of "cores", areas of myofibrillar disruption and reduced mitochondrial activity. Subtypes include Central Core, Multi-Minicore and Core Rod Myopathies [1]. A recently identified form, Dusty Core Disease (DuCD), is distinguished by irregular, undefined myofibrillar disorganization, reddish-purple granular deposits, patchy oxidative enzyme staining, and absence of ATPase activity [2]. DuCD has been associated only with recessive *RYR1* variants, severe early onset phenotypes and reduced RyR1 protein in muscle [2–4].

The *RYR1* gene encodes the skeletal muscle ryanodine receptor 1, which forms a homotetrameric calcium-release channel in the sarcoplasmic reticulum. This channel establishes contact with DHPR (dihydropyridine receptor) in the triad, a muscle-specific region, essential for excitation-contraction coupling [5–7].

RYR1 variants associated with Central Core Disease (CCD) and Malignant Hyperthermia (MH) are mainly found in three "hot spot" domains: N-terminal (residues 1–614), central region (2163–2458), and C-terminal (4136–4973) [8]. Nevertheless, recent findings show that variants causing a dominant disease can occur throughout the entire gene [9]. *RYR1* variants can result in channel gain- or loss-of-function, RyR1-DHPR coupling modification, or RyR1 global reduction, resulting in decreased calcium release and muscle weakness [10, 11].

This study characterizes four DuCD patients by clinical, pathological and genetic perspectives, highlighting heterogeneous phenotypes ranging from recessively inherited severe early-onset forms to dominantly inherited adult-onset cases with moderate disease. Histological, ultrastructural and immunohistochemical techniques were employed to investigate myopathology underlining these presentations and to expand understanding of DuCD and its hereditary patterns.

MATERIALS AND METHODS

Patients

This study involved two adults and two pediatric subjects in compliance with ethical standards, national legislation and institutional guidelines. All participants provided written informed consent to undergo for muscle biopsy, blood sampling and clinical data collection. Study protocol was approved by the local Ethical Committee.

Muscle biopsy

Haematoxylin and Eosin (H&E, Bio-Optica, Milano, Italy) and Modified Gömöri Trichrome (MGT, Bio-Optica) stains were performed on 8 µm-thick cryostat

[1]Department of Neuroscience, Foundation IRCCS Ca' Granda Ospedale Maggiore Policlinico, Neuromuscular and Rare Diseases Unit, Milan, Italy. [2]Department of Neuroscience, Foundation IRCCS Ca' Granda Ospedale Maggiore Policlinico, Neurology Unit, Milan, Italy. [3]Dino Ferrari Centre, Department of Pathophysiology and Transplantation (DEPT), University of Milan, Milan, Italy. [4]Unit, University Hospital, Azienda Ospedaliera Universitaria Integrata, Verona, Italy. [5]Department of Neurosciences, Biomedicine and Movement Sciences, University of Verona, Verona, Italy. [6]IRCCS Bambino Gesù Children Hospital, Translational Cytogenomics Research Unit, Laboratory of Medical Genetics, Rome, Italy. [7]IRCCS Eugenio Medea, Neurorehabilitation Dept, Unit of Rare Diseases of the Central and Peripheral Nervous System, Bosisio Parini, Lecco, Italy. [8]The NEMO Center in Milan, Neurorehabilitation Unit, University of Milan, ASST Niguarda Hospital, Milan, Italy. [9]Department of Precision Medicine, University of Campania "Luigi Vanvitelli" and Telethon Institute of Genetics and Medicine (TIGEM), Naples, Italy. ✉email: daniela.piga@policlinico.mi.it

Received: 8 August 2025 Revised: 2 February 2026 Accepted: 24 February 2026
Published online: 18 March 2026

muscle sections. On H&E-stained sections, fibers with nuclear centralization were counted as percentage on total fibers and the fibrotic area was quantified using Leica Application Suite 4.9.0 and ImageJ 1.53c software. Morphological analysis also included myosin ATPase (pH 9.4 - 4.6 - 4.3), cytochrome c oxidase (COX), succinate dehydrogenase (SDH), acid phosphatase (AP), NADH dehydrogenase staining (all reagents from Sigma-Aldrich, St. Louis, Mo, USA).

Genetic analysis

All patients were tested using Congenital Myopathy gene panels and the data were analyzed using standard bioinformatic methods. Variants without effect were excluded and while the others were filtered using Ensemble, LOVD, dbSNP database. Allele frequency was assessed by Exome Variant Server and gnomAD database. Pathogenicity was evaluated by SIFT, PolyPhen-2, Mutation Taster and ACMG classification. Rare variants were confirmed by Sanger re-sequencing (3130 Genetic Analyzer, Applied Biosystems, Waltham, MA, USA). Genotype-phenotype relationships were searched through Pubmed, ClinVar, OMIM and Genetable database. Splicing variants were assessed by SpliceAI and Human Splicing Finder.

For *CACNA1S* and *RYR1* splicing analysis, total muscle RNA was extracted using TRIzol (Invitrogen Life Technologies, Carlsbad, California, USA), it was retrotranscribed with Transcriptor High Fidelity cDNA Synthesis kit (Roche, Basel, Switzerland) and cDNA was sequenced by Sanger.

Western blot

Muscle homogenates (40 µg) from patients and age-matched controls were electrophoresed on 5% acrylamide and transferred onto LF-PVDF membranes (Bio-Rad, Hercules, CA, USA). Membranes were probed with anti-RYR1 (1:4000 mouse monoclonal; Invitrogen Life Technologies, Waltham, MA, USA), anti-DHPR (anti-CACNA1S 1:450 mouse monoclonal, Abcam, Cambridge, UK). α-actinin-1 (1:4500 mouse monoclonal, Sigma-Aldrich, Burlington, MA, USA) was used for normalization and IRDye 800CW as secondary antibodies (1:18000; Li-Cor Biotech, Lincoln, NE, USA). Immunobands were developed with Odyssey Fc Imaging System (Li-Cor Biotech) and were quantitated densitometrically as arbitrary unit (AU) using n-Image Studio Software (Li-COR Biosciences, Bad Homburg, Germany).

Statistical analysis

Statistical analysis on three different experiments was performed using GraphPad Prism 10.1.0 (GraphPad Software Inc., LaJolla, CA, USA). Data were expressed as mean ± SD with significativity set at $p \leq 0.001$ (**) and $p \leq 0.05$ (*). Difference between patients and controls was assessed with Wilcoxon–Mann–Whitney test.

Immunofluorescence staining

Muscle cryosections were fixed and blocked with normal goat serum (Vector Laboratories, Newark, CA, USA). The following antibodies were used: RYR1 (1:1000, mouse monoclonal; Invitrogen Life Technologies), DHPR (anti-CACNA1S 1:100, mouse monoclonal, Abcam), desmin (1:100 mouse monoclonal; Chemicon, Millipore, Billerica, MA, USA), αB-crystallin (1:100 rabbit polyclonal; Chemicon), myotilin (1:10, mouse monoclonal, Novocastra, Nussloch, Germany), MHC-1 (anti-Myosin Heavy Chain, monoclonal antibody FITC-coniugated, 1:50 Miltenyi Biotech, Bergisch Gladbach, Germany). Perlecan (1:200 rat monoclonal, Sigma-Aldrich) was used as membrane marker. Goat anti-mouse Alexa-488 or goat anti-rabbit Alexa-596 (1:1000; Thermo Fisher, Waltham, MA, USA) was used as secondary antibody. Slides were mounted in Vectashield anti-fade mounting medium containing DAPI (Vector Laboratories, Burlingame, CA, USA) for nuclei counterstaining.

Electron microscopy

Tiny muscle specimens were fixed in 2.5% glutaraldehyde (Electron Microscopy Sciences EMS, Hatfield, PA, USA) and post-fixed in 2% osmium tetroxide. Next, they were ethanol-dehydrated and embedded in Epon. Ultrathin sections, prepared using Power Tome XL ultramicrotome (RMC, Tucson, AZ, USA) were stained with lead citrate and uranyl acetate, and examined with a Hitachi HT7800 transmission electron microscope (Hitachi, Japan).

RESULTS

Clinical aspects

The four patients presented heterogeneous phenotypes ranging from severe childhood-onset forms to milder adult-onset presentations. Three cases had no family history, whereas one subject (Pt1) came from a family with four affected members (Table 1).

Patient 1. This mid-forties female showed congenital hip dysplasia, delayed motor milestones, severe scoliosis and fatigability with reduced global motor performance from childhood. Muscular weakness slowly, but progressively worsened over the years, more evidently so in the lower limbs. She presented a myopathic face, rhinolalia without dysphagia, mild hypotonia and proximal-distal weakness at four limbs. She showed difficulty in climbing stairs and getting up from a sitting or squatting position. Standing posture was maintained with a slightly widened base; she had right-convex dorsal scoliosis, increased dorsal kyphosis and mild lumbar hyperlordosis with anterior pelvic tilt. Gait was limited by reduced lifting of the forefoot, though without clear steppage. Clinically, the most involved muscles were *triceps brachii*, iliopsoas and *tibialis anterior* (Medical Research Council scale or MRC, 3–3.5 bilaterally). She denied muscle cramps or myoglobinuria. Electromyography (EMG) showed a myopathic pattern. Creatine kinase (CK) levels (138 U/L), cardiology assessment and nocturnal oximetry were normal. Overall, her clinical phenotype could be considered moderate. Three more family members were affected with variable clinical course associated to the same haplotype.

Patient 2. This middle-aged man had a three-year history of proximal weakness and fatigability. EMG showed a myopathic pattern and muscle magnetic resonance imaging (MRI) confirmed muscle damage in the four limbs and axial compartment. More specifically, muscle MRI did not show significant atrophy, but detected signs of fibro-adipose infiltration. This was more prominent in the adductor longus (right greater than left, fat fraction 45%), as well as in the soleus and medial gastrocnemius muscles bilaterally. Milder fibro-adipose infiltration involving the paraspinal muscles, the distal portion of the vastus intermedius and, in the upper limbs, the subscapularis, teres major, and latissimus dorsi muscles, was also observed. Serum CK level was mildly elevated (552 U/L). Neurological evaluation showed hypophonia, severe weakness of neck muscles with head drop, and proximal weakness of the four limbs (4/5 at MRC) with waddling gate and dorsal kyphosis. Voluntary arm abduction was limited to 90 degrees. He could walk on his toes and heels. The overall clinical presentation was moderate. No family history was reported.

Patient 3. This little girl was severely affected, indeed, she had congenital arthrogryposis, scoliosis and progressive muscle weakness. She achieved normal milestones for sitting and crawling, but required support to stand, which she attained at 3 years. She underwent surgery for ankle and hip retractions. When evaluated, she showed severe proximal muscle weakness with retractions and was wheelchair-dependent even if she could stand with orthesis. She had a severe left-convex thoracolumbar scoliosis with pelvic rotation, dorsal kyphosis and lumbar lordosis with right lower costosternal prominence. She denied dysphagia. Cardiological evaluation was normal, whereas respiratory assessment detected a mild restrictive pattern, which required non-invasive ventilation 2 h daily. EMG studies performed shortly after birth showed myopathic signs. CK values measured the day after birth following acute tachypnea, were significantly increased (10792 U/L), but subsequently spontaneously normalized and remained normal thereafter. A likely perinatal trauma was considered responsible for the temporary enzymatic increase. Muscular MRI showed severe symmetric fibro-adipose substitution of the gluteus maximus, the anterior thigh compartment and the lateral leg compartment. She had no family history.

Patient 4. This little girl was adopted in early childhood along with two older healthy siblings. No family information is available.

Table 1. Clinical and molecular findings in the investigated patients.

Patient/ sex	Age range (years)	Phenotype	RYR1 genetic variant	Protein alteration/ domain	Functional regions	Validation	Variant classification (ACMG)	Note
1/F	40-50	• Clinical severity: moderate • Congenital hip dysplasia • Delayed motor milestones • Myopathic face • Mild hypotonia • Proximal weakness starting in childhood • Severe scoliosis • Fatigability • CK: 138 U/L • EMG: moderate myogenic pattern	c.14678G>A het (Ex 102)	p.Arg4893Gln Pore	CCD hotspot 3	Family segregation: dominant transmission [12, 16–18]	Likely pathogenic: PP3-PM2-PM5-PP2	Presence of an additional variant *in cis* in *RYR1* (c.8327C>T p.Ser2776Phe het Domain RYR3-4) linked to MH [31, 32]
2/M	50–60	• Clinical severity: moderate • Late onset (50 yrs) • Head drop • Mild hypophonia • Proximal weakness • CK: 522 U/L • EMG: myogenic-neurogenic pattern	c.7600G>A het (Ex 47)	p.Ala2534Thr Bsol	Critical region for skeletal-type E-C coupling (1635–2636)	NA	VUS: PM2-PP2	New variant (this report)
3/F	<10	• Clinical severity: severe • Congenital arthrogryposis • Scoliosis • Delayed motor milestones • Proximal weakness • Wheelchair dependent • Restrictive respiratory pattern • CK: normal (10792 U/L at birth) EMG: myogenic pattern	c.131G>A hom (Ex2)	p.Arg44His NTD-A	MH/CCD hotspot 1	Family segregation: recessive transmission [12, 13]	Likely pathogenic: PP3-PM2-PM5-PM1-PP2-PS4	
4/F	<10	• Clinical severity: severe • Delayed motor milestones • Pectus excavatum • Ophthalmoparesis • Moderate proximal weakness • Recurrent lung infections • CK: normal • EMG: myogenic pattern	c.325C>T het (Ex4) c.13622del het (Ex 93)	p.Arg109Trp NTD-A p.Phe4541Serfs*10 Link-pVSD	MH/CCD hotspot 1 Important region for activation/ inactivation (aa 4300–4850)	Expression studies in HEK cells [14, 15] Loss of function	Pathogenic: PM3-PP3-PM2-PM5-PP2-PS3-PP1-PP5 Likely pathogenic-PVS1-PM2	New variant (this report)

Clinical phenotype, genetic and protein variants of patients. RYR1 RefSeq: NM_000540.3 (NP_000531.2).
ACMG American College of Medical Genetics and Genomics, *CK* Creatine Kinase, *EMG* electromyography, *E-C coupling* Excitation-Contraction coupling.

We only know that her mother suffered cytomegalovirus infection and toxoplasmosis during pregnancy and that she presented hypotonia and poor sucking at birth. She was diagnosed at the age of 4 years because of delayed motor milestones and frequent respiratory tract infections. Neurological examination showed moderate facial weakness, external ophthalmoparesis, pectus excavatum and proximo-distal limb weakness. She was able to rise to standing using Gowers' manoeuvre and could walk unsupported. EMG was myopathic in both proximal and distal muscles (examined muscles: deltoid, *biceps brachii*, first dorsal interosseus of the hand, *vastus lateralis* and *tibialis anterior*) and serum CK levels were normal. Due to compression of underlying organs (reduced caliber of the left main bronchus, compressed heart in particular right atrium, proximal esophageal ectasia, reduction of tracheal caliber at the passage of the innominate artery) she underwent sternochondroplasty surgery before the age of five years, with no complications. The clinical picture gradually improved over the years and now she is still ambulant, with mild dysphagia and respiratory restrictive syndrome.

Molecular analysis

Using the Next Generation Sequencing analysis, we identified four subjects carrying *RYR1* variants (NM_000540.3) and displaying myopathological features compatible with Dusty Core Disease: two pediatric cases (Pt3 and Pt4) presented recessive disease inheritance, whereas two adult patients (Pt1 and Pt2) had heterozygous causative defects with clear dominant inheritance only for Pt1. DNA samples for segregation studies were obtained only from relatives of Pt1 and Pt3. Five detected *RYR1* variants proved to be rare molecular defects (gnomAD MAF < 1%). Specifically, the c.7600G>A variant (Pt2) displayed an extremely low allele frequency, whereas the c.13622del variant (Pt4) was absent from gnomAD; neither genetic alteration had been reported in previous studies.

The previously described nucleotide changes c.131G>A (Pt3) [12, 13], c.325C>T (Pt4) [14, 15] and c.14678G>A (Pt1) [12, 16–18] were localized in RYR1 mutational hotspots linked to CCD and impacted the NTD-A (c.131G>A, c.325C>T) and Pore (c.14678G>A) domains. The novel missense change c.7600G>A, found in Pt2, was located in a critical region for skeletal muscle excitation-contraction coupling. cDNA analysis in skeletal muscle ruled out any aberrant splicing or transcript instability. The microdeletion c.13622del in Pt4 likely produced a frameshift introducing a premature stop codon p.Phe4541Serfs*10. cDNA sequencing from muscle tissue showed that the transcript carrying this variant was partially absent, suggesting an almost complete nonsense-mediated mRNA decay.

Two patients displayed additional genetic alterations. In Pt1 we found a further *RYR1* nucleotide change, c.8327C>T, previously associated with MH, which was *in cis* with c.14678G>A. In Pt2 we observed the heterozygous intronic variant c.398+3G>A in *CACNA1S* (NM_000069): cDNA analysis ruled out splicing alteration (data not shown).

All main features of each genetic defect are reported in Table 1.

Protein studies

Western blot analysis on RYR1 and DHPR showed different expression levels among patients. Densitometric quantification of RYR1 normalized versus actinin displayed a significant reduction for Pt1 (28.49% ± 0.43%), Pt3 (5.56% ± 0.38%) and Pt4 (51.34% ± 1.4%), while Pt2 expressed a normal value (107.24% ± 4.36%). Expression levels of DHPR resulted variably reduced in all patients: 27.03% ± 3.18% in Pt1, 46.88% ± 12.47% in Pt2, 16.87% ± 9.2% in Pt3 and 60.97% ± 5.52% in Pt4 (Fig. 1).

Morphological findings

Histological evaluation of muscle biopsies showed marked fiber size variability with type 1 fiber hypotrophy, increased number of fibers with internalized myonuclei and myopathic changes, namely the increase in connective and adipose tissue (Fig. 2, Table 2).

Patient 1. Brachial biceps muscle biopsy revealed moderate fiber size variability characterized by scattered hypotrophic fibers. A mild increase in peri- and endomysial connective tissue was quantified at 12% (30,26% fat and 69,73% connective) while the percentage of fibers with internalized myonuclei was 18%. NADH enzymatic activity staining showed numerous muscle fibers containing focal areas devoid of enzymatic activity. In some fibers, single, well-circumscribed circular regions of reduced staining were identified, located either at intracytoplasmic or at subsarcolemmal level. Other fibers exhibited multiple, irregularly distributed foci of diminished NADH activity throughout the cytoplasm.

MTG showed deposition of reddish-purple granular material in some fibers. ATPase staining at pH 4.3 and MyHc slow immunofluorescence showed a fiber type uniformity for the selective presence of type I fibers (Additional file 1: Supplementary Fig. S1).

Patient 2. He underwent a brachial biceps muscle biopsy, which revealed discrete fiber size variability caused by the presence of several hypotrophic fibers. A mild increase in peri- and endomysial connective tissue was quantified at 16% (32.84% fat and 67.15% connective tissue) while the percentage of fibers with internalized myonuclei was 12%. NADH activity was heterogeneously distributed, several fibers showing areas of central cytoplasmic rarefaction without round or ovoidal shape ("core-like" areas). No granular reddish material was observed with MGT. pH 9.4 ATPase showed a normal fiber type differentiation with predominance of type 2 fibers. Hypotrophic fibers predominantly belonged to type I. This data was confirmed by MyHc slow immunofluorescence (Additional file 1: Supplementary Fig. S1).

Patient 3. A brachial biceps muscle biopsy showed a consistent amount of fibrotic tissue (38% totally: 8.66% fat and 91.33% connective tissue) and a moderate fiber size variability with type I predominance. The latter was confirmed by pH 4.3 ATPase staining and by MyHc slow immunofluorescence even if the quality of the tissue was not optimal for immunofluorescence studies (Additional file 1: Supplementary Fig S1). The percentage of fibers with internalized myonuclei was 17%. NADH activity was non-homogeneously distributed in all fibers, many of them showing multiple areas of central, "core-like" cytoplasmic rarefaction. MGT staining showed the presence of reddish-purple granular materials deposition both inside and outsides core area.

Patient 4. A quadriceps skeletal muscle biopsy revealed prominent fiber type disproportion, type I fibers being more numerous and almost all hypotrophic, a data confirmed by MyHc slow staining (Additional file 1: Supplementary Fig. S1). Connective and adipose tissues were mildly increased (14%: 18.54% fat and 81.45% connective tissue), whereas the percentage of fibers with internalized myonuclei was 8%. NADH activity was centrally rarefied in several type 2 fibers, with occasional "targetoid" appearance in type 1 fibers. No granular reddish material was observed with MGT.

Immunofluorescence analysis

The analysis showed both RYR1 and DHPR positivity in core areas, but with different intensity and distribution. In Pt1 and Pt3 we detected a positive signal for RYR1 and DHPR in association with core areas. Pt4 showed a peculiar aggregation of DHPR in some fibers, indeed, in this patient, the signal intensity was higher than in the other cases. Furthermore, the immunoreactivity was mainly

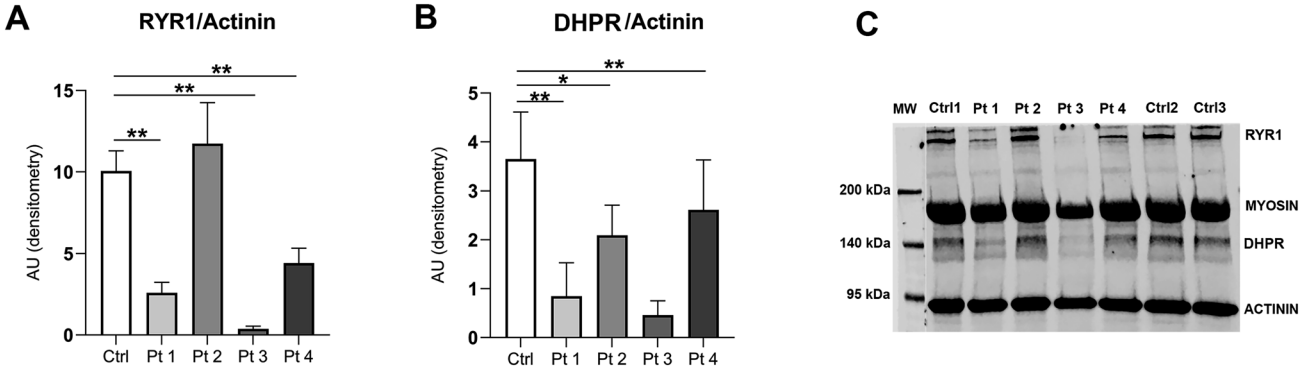

Fig. 1 Western blot. Densitometric quantification of RYR1 (**A**) and DHPR (**B**) after normalization on actinin. $N = 3$. **C** Representative blot. Significance was set at $p \leq 0.001$ (**) and $p \leq 0.05$ (*).

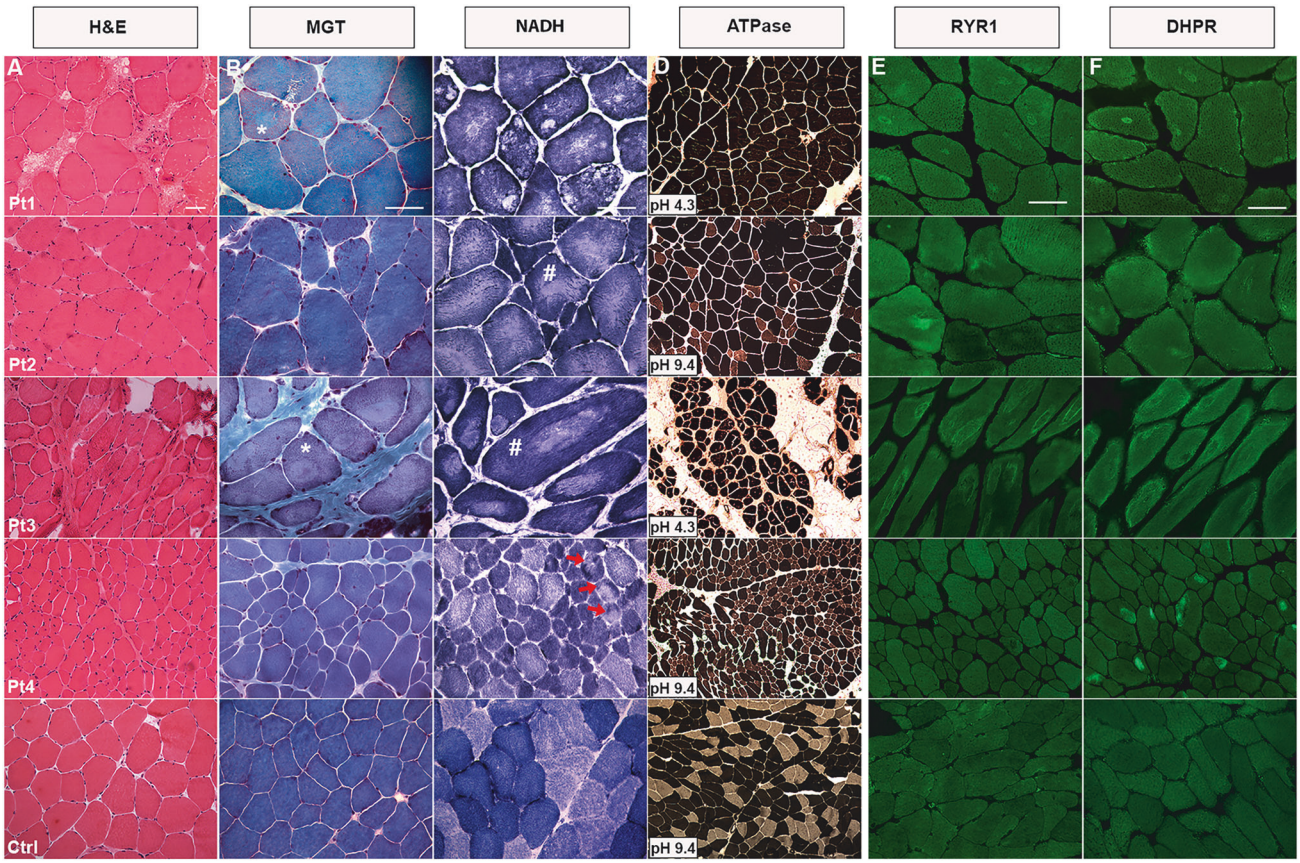

Fig. 2 Muscle biopsy findings. H&E (**A**), MGT (**B**), NADH activity (**C**) and ATPase staining at pH 9.4 or 4.3 (**D**) from patients and control. Asterisks (*) indicates reddish-purple granular materials. Hashtags (#) mark dusty core area. Red arrows point to NADH activity with "targetoid" appearance. Scale bar 50 µm. RYR1 (**E**) and DHPR (**F**) immunofluorescence staining in patients and control. Scale bar 50 µm.

located in the subsarcolemmal area of the muscle fibers. No significant RYR1 positivity was observed. In Pt2, some muscle fibers showed a RYR1 positivity, but this was not strictly limited to the central core areas. A similar, but less marked signal distribution was observed for DHPR in few fibers (Fig. 2E, F).

The signal of αB-crystallin, desmin, myotilin was altered due to the tendency to form aggregates, that in some fibers showed a core-like deposition. In Pt4, the deposition of αB-crystallin and myotilin differed from the other patients, indeed, signal positivity was localized in the peripheral area of the fibers (Fig. 3A–D). In all patients αB-crystallin and myotilin showed an almost complete colocalization.

The main features are reported in Table 2.

Electron microscopy

Ultrastructural examination revealed several important alterations, namely regions of sarcomeric disorganization of variable size, shape and distribution. These abnormalities were distributed both among and within individual fibers, some areas showing well-preserved sarcomeres adjacent to markedly altered regions (Fig. 4). Two main structural abnormalities were consistently identified within the affected fibers. The first consisted of electrondense, longitudinally smeared Z-line, extending over several sarcomeres and forming irregular, elongated densities along the myofibrillar

Table 2. Histological, ultrastructural and protein studies in patients' muscle biopsies.

Patient	Muscle biopsy	Biopsy (age range at biopsy)	MGT	NADH	IF RYR1/DHPR	IF αBcryst/Desm/Myot	Electron microscopy	Western Blot (% residual expression)
1	Biceps brachii	Central Core Myopathy (30–40 y)	Reddish purple granular material deposition	Mini cores with irregular areas, without clear borders and round/ovoidal shape Mouth-eaten fibers, myofibrillar disruption	Positive signals in core areas with widespread deposits of RYR1 and DHPR	Myofibrillar aggregates or thickening, that in some fibers show a core-like deposition	Some small areas of sarcomeric disorganization characterized by thickening of z-line	RYR1: 28.49 ± 0.43 DHPR: 27.03 ± 3.18
2	Biceps brachii	Central Core Myopathy (50–60 y)	Very low deposition of reddish-purple granular material	In most fibers presence of irregular core areas without clear borders and round/ovoidal shape	Positive signals in core areas with different intensity and distribution	Widespread myofibrillar deposits	Areas of sarcomeric disorganization with abundant electrodense longitudinally smeared material and thickened short Z-line fragments. Multiple core areas may be present within the same fiber	RYR1: 107.24 ± 4.36 DHPR: 46.88 ± 12.5
3	Biceps brachii	Central Core Myopathy (<10 y)	Presence of reddish-purple granular material deposition inside and outside core areas	Presence of extensive and more regular core areas without clear borders	Positive signals in all core areas with more evident aggregates of RYR1 and DHPR	More evident myofibrillar aggregates or thickening, that in some fibers show a core-like deposition	Large core areas, sometimes showing irregular network of myofilaments with mild Z-line thickening and fragmentation in some fibers	RYR1: 5.56 ± 0.38 DHPR:16.87 ± 9.2
4	Quadriceps	Fiber Type Disproportion (<10 y)	Presence of mild and small reddish-purple deposition in few core areas	Fibers with core-like areas without clear borders Some fibers with "targetoid" appearance	Positive signals in core areas with different intensity and distribution Some fibers with accumulations of DHPR	Myofibrillar aggregates in some fibers	Core areas of variable size, irregular network of myofilaments and Z-line thickening	RYR1: 51.34 ± 1.4 DHPR: 60.97 ± 5.52

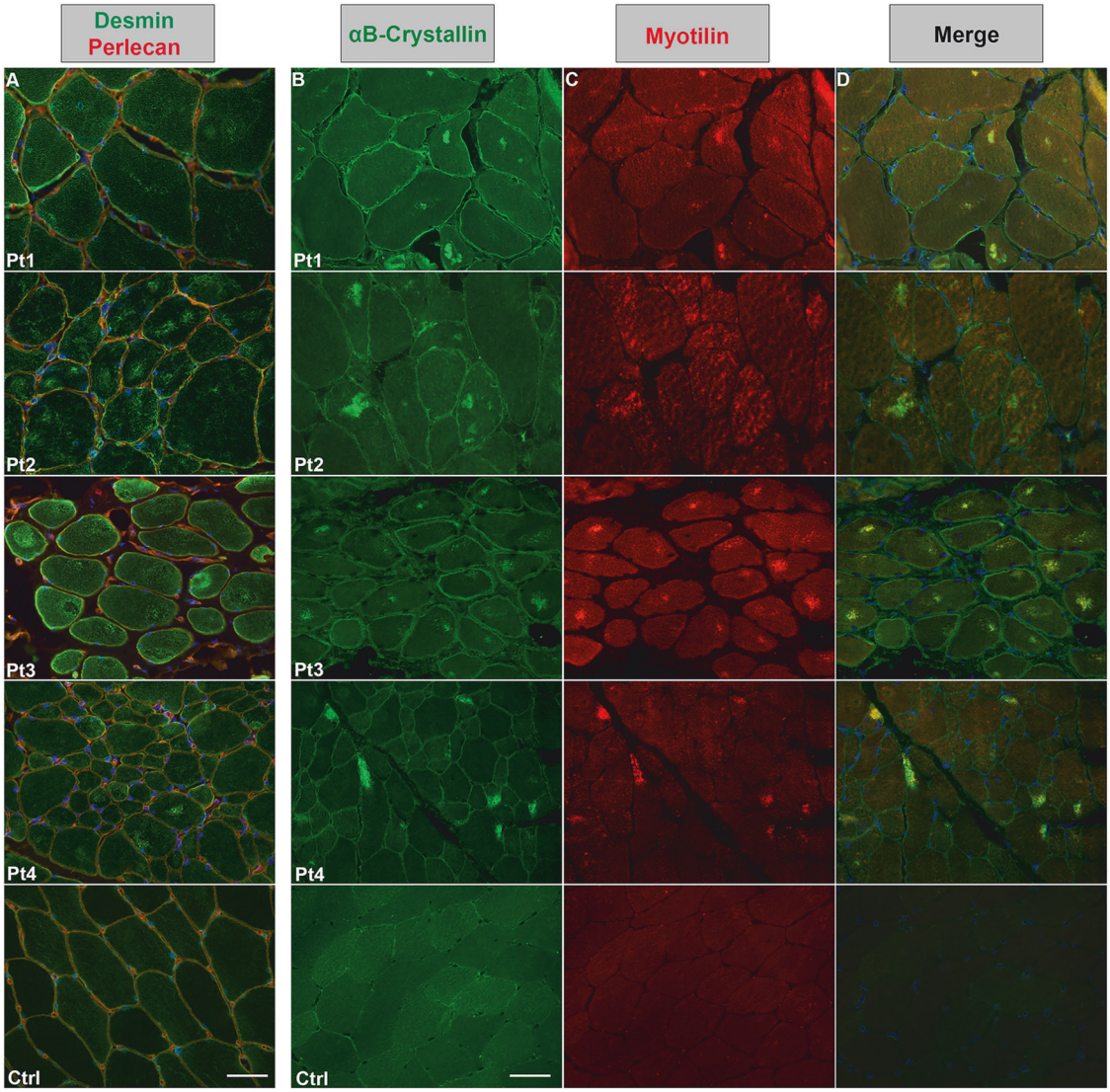

Fig. 3 Immunofluorescence staining. Altered expression and deposition of desmin (**A**), αB-crystallin (**B**), and myotilin (**C**) in both patients and control. **D** Merge channel. Perlecan for membrane staining and DAPI for nuclei counterstaining. Scale bar 50 µm.

axis (Fig. 4B–D). The second type of alteration was represented by thickened and fragmented Z-line segments of reduced length, often appearing discontinuous and associated with an irregular network of myofilaments (Fig. 4A). The degree of Z-line fragmentation varied, ranging from mild irregularities to nearly complete disruption of the normal transverse alignment.

In some fibers, the disorganization spanned the entire fiber width, forming broad or elongated core regions. In longitudinal sections, these elongated cores extended for up to 15–20 sarcomeres (Fig. 4G). Multiple core areas were frequently observed within single fibers, either as isolated regions or as larger zones of sarcomeric disruption (Fig. 4C and Additional file 2: Supplementary Fig. S2A). Mitochondrial were completely absent in all core areas (Additional file 2: Supplementary Fig. S2C). Subsarcolemmal core areas were also detected (Fig. 4F and Additional file 2: Supplementary Fig. S2D). Also, additional minor alterations were observed, specifically mild Z-line streaming and focal areas of partial myofibrillar disorganization (Additional file 2: Supplementary Fig. S2B). These subtle changes were frequently interspersed with regions of normal structure. In Pt4, these highly disorganized regions also contained membrane stacks [4], extending over several micrometers (Table 2, Fig. 4H, Additional file 3: Supplementary Fig S3).

DISCUSSION

We describe the clinical, genetic and pathological features of four Italian DuCD patients. These probands, more specifically three isolated cases and one subject from a family with three other affected relatives, were identified in our Congenital Myopathy cohort. They present heterogeneous phenotypes including both severe autosomal recessive (AR) early-onset cases (Pt3 and Pt4) and less severely affected autosomal dominant (AD) adult-onset forms (Pt1 and Pt2). Dusty Core Disease is reported as the most common histopathological presentation of myopathies due to *RYR1*-recessive mutations [2, 19]. Our finding of two likely AD RYR1 forms, characterized by DuCD typical histopathological features, therefore enlarges the knowledge on the hereditary pattern of this Core Myopathy subgroup. Due to the diagnostic complexity associated to the validation of *RYR1* variants, we employed different histological, immunological and ultrastructural techniques to support the pathogenic role of the identified variants in the apparently AD cases.

The combined use of ACMG criteria [20, 21] and our experimental evidence allowed the classification of all identified variants as pathogenic or likely pathogenic. In particular, we propose a revised reclassification for c.14678G>A and c.13622del, upgrading from

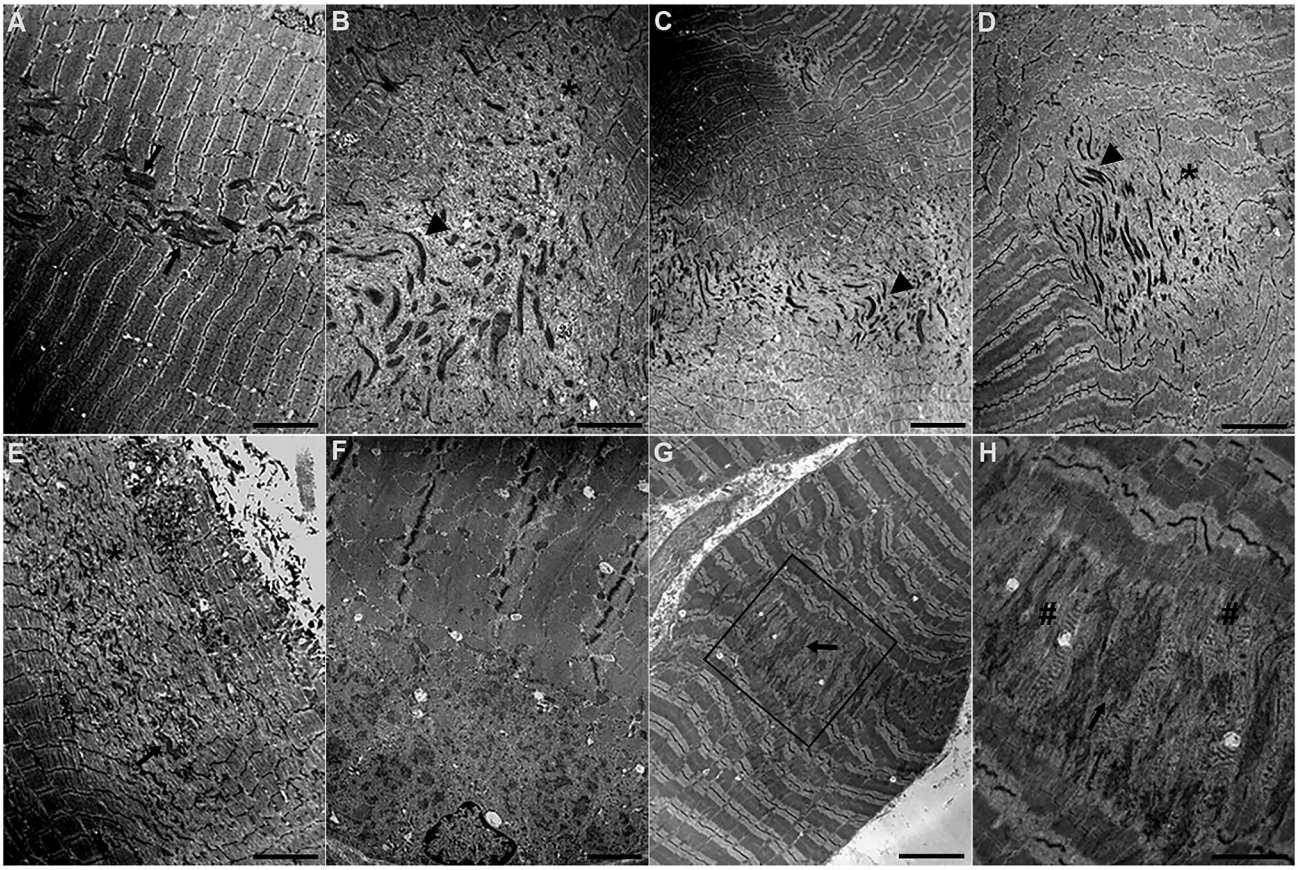

Fig. 4 Ultrastructural analysis. Representative electron microscopy (EM) images from patients 1 (**A**), 2 (**B**–**D**), 3 (**E**), and 4 (**F**–**H**), showing sarcomeric disorganization of varying sizes. Arrows indicate thickened Z-lines, arrowheads smeared Z-lines and asterisks short Z-line fragments. Multiple core areas are visible within single muscle fibers (**C**). Hashtags (#) indicate membrane stacks. Panel (**H**) is a high-magnification view of the boxed region in panel (**G**). Scale Bar (**A**, **B**, **D**, **E**, **G**: 5 µm; **C**, **F**: 2,25 µm; **H**: 2 µm).

likely pathogenic to pathogenic, and of the c.7600G>A variant, upgraded from variant of uncertain significance to likely pathogenic (Additional file 4: Supplementary Table 1).

Among our subjects, Pt3 presented the typical DuCD genotype-phenotype association, indeed, she showed a severe phenotype linked to a homozygous missense mutation in the important functional domain NTD-A, involved in the stabilization of MIR folding domain [2, 22]. The morphological evaluation demonstrated the prevalence of type I fibers characterized by the deposition of reddish-purple granular material in core areas, sometimes multiple, that appeared ultrastructurally elongated with Z-line thickening and fragmentation, often associated with irregular myofilament network. The myofibrillar alteration was confirmed by the presence of desmin, myotilin and αB-crystallin aggregates, showing a core-like localization. In addition, as reported in literature, there was an alteration in the expression and distribution of RyR1 and DHPR, that resulted extremely reduced and aggregated at the level of core area [2, 4].

Dusty cores in DuCD patients can be morphologically heterogeneous, ranging from large sarcomeric disorganization areas to small subsarcolemmal or cytoplasmic spots. In addition, some cases have been reported in which dusty cores were present only in few fibers, and were thus underestimated, or appeared only late in life [2]. This was the case of Pt4, whose morphological analysis did not reveal any reddish-purple granular material, but exclusively few fibers with a "targetoid" appearance.

Further DuCD confirmation in Pt 4 came from the ultrastructural investigation, showing the presence of highly disorganized sarcomeric regions, occasionally spanning the entire fiber width and containing Z-line thickening and large membrane stacks, similar to those described in literature [2, 4]. Regarding their possible significance, multiple membrane stacks, observed in response to reduced RYR1 expression, were thought to originate from T-tubule and sarcoplasmic reticulum (SR) membranes, i.e., components of the triad [4]. This likely represents an adaptive response to increased junctional surface and RyR1 density, preserving Ca^{2+} release despite reduced SR storage.

Subsarcolemmal and intrafibral core areas were immunohistochemically characterized by an altered network of myofilaments with the particular deposition of myotilin and αB-crystallin, that differed for their major localization in the peripheral fiber areas. Immunostaining and western blot analysis showed a halving of RyR1 and DHPR expression and a peculiar DHPR aggregation in some fibers. These features associated with clinical and genetic data pointed to a possible severe recessive case of DuCD.

For Pt1 and Pt2, carrying single heterozygous variants of *RYR1*, we applied a combination of diagnostic tools to define the pathogenicity of these molecular alterations and their possible association with the DuCD. Our patients are interesting not only for the presence of dusty cores, associated with a moderately severe phenotype, but also for their peculiar genetic presentation.

Pt2 caught our attention because of the presence in most fibers of a particularly heterogeneous NADH activity distribution, defined by core areas without round/ovoidal shape and clear borders, very different from the classical central core staining. The ultrastructural analysis suggested a DuCD because the altered fibers turned out to contain multiple core areas with variable sarcomeric disorganization, also quite extended, characterized by short thickened

fragments of the Z line and copious electrodense longitudinally smeared material, similar to those described by Garibaldi and colleagues [2]. In the patient's biopsy there was also a widespread irregular deposition of the myofibrillar network, which is an additional, already described feature of the fibers with dusty cores. The genetic analysis of this patient is quite peculiar because we found a heterozygous variant in *RYR1* (c.7600G>A, p.Ala2534Thr), which causes a protein alteration in a critical region for excitation-contraction coupling in skeletal muscle, and also a single splicing site alteration in *CACNA1S*. Expression studies showed a reduction in the DHPR protein level, but a normal RyR1 production, even if both showed a similarly altered distribution, not clearly restricted to dusty cores. In recent years, the increasing use of the Next Generation Sequencing through the analysis of gene panels has led to the discovery of an ever-increasing number of subjects carrying coexisting pathogenic variants in skeletal muscle channelopathies [23]. Causative loss- and gain-of-function variants in *CACNA1S* have also been described in association with core myopathies, but patients' biopsies presented different histological features characterized by an intermyofibrillar network displaying an "alveolar" aspect [24]. To clarify whether RYR1 or CACNA1S caused the pathology, we analyzed CACNA1S RNA splicing. No alteration was found, supporting the pathogenic role of the RYR1 variant. Therefore, in our opinion the presence of an altered expression and distribution of DHPR is due to the RyR1 pathogenic variant that is located in an important region for bi-directional coupling with DHPR [24, 25]. Moreover, in skeletal muscle the EC coupling is ensured by multiple physical interactions and a tight geometrical alignment between DHPR and RyR1, but also by the presence of other core components as STAC3 (SH3 and cysteine rich domain 3) and junctophilin2 [26, 27]. Therefore, in our patient the alteration in RyR1 distribution likely compromises the correct DHPR localization and, consequently, the stability of the entire skeletal excitation contraction coupling machinery, leading to a profound alteration of the sarcomeric structure, namely the formation of dusty core-like structures in the muscle fibers.

We identified another interesting case (Pt1) with irregularly shaped multi-minicores at morphological analysis, which, however, showed some reddish-purple granular material deposition similar to that described for DuCD [2]. An additional confirmation of our hypothesis was the presence of small ultrastructural areas with thickening of z-line and myofibrillar disorganisation, probably due to an altered deposition of myotilin, αB-crystallin and desmin. Interestingly, WB analysis disclosed a markedly reduced expression of RyR1 and DHPR, whereas at the immunostaining some fibers showed a core-like accumulation similar to the distribution observed in the *RYR1* recessive Pt3. However, the peculiarity of Pt1 is the presence of two dominant alterations segregating *in cis*, the c.14678G>A heterozygous pathological variation associated with CCD and the c.8327C>T substitution linked to HM (Table 1). Nowadays, two families with a double RYR1 mutation in the same allele have been described and, in both cases, the associated phenotype was Multiminicore Myopathy and Malignant Hyperthermia susceptibility. The histochemical and ultrastructural findings in the muscle biopsy of these cases were very similar to those observed in our patient [28, 29]. Pt1's genetic alterations have been reported several times, but no functional studies have ever been published; therefore, we studied Pt1 intracellular calcium variations to evaluate the functional effect due to the co-presence of these two variants, and observed an altered sensitivity of Pt1 myoblasts to caffeine concentrations, which suggests an altered activation threshold of the RyR1 channel (Additional file 5).

This study expands the understanding of DuCD by describing four Italian patients with different clinical, genetic and histopathological outcomes. The identification of severe early-onset recessive and less severe adult-onset dominant cases reinforces the heterogeneity of RyR1-related myopathies. Particularly, the presence of DuCD-specific histopathological features in dominant *RYR1* cases broadens the knowledge about the inheritance patterns of this disease subgroup. Furthermore, the RYR1 and DHPR molecular expression observed in our patients confirms and reinforces the relation between these proteins. Indeed, pathogenic *RYR1* variants, either loss- or gain-of-function, resulting in reduced protein expression or in alterations of critical EC-coupling domains, were also associated with a concomitant downregulation of the DHPR α 1 subunit, focal accumulations of both proteins within or around dusty-cores, and a marked disruption of the spatial organization of the EC-coupling machinery [6, 30].

Overall, this study expands the current understanding of Dusty Core Disease by demonstrating that DuCD is not exclusively a recessive RYR1-related condition. The identification of two adult-onset cases carrying heterozygous dominant pathogenic variants, but showing unequivocal DuCD morphological features, reveals that the disease can be both recessively and dominantly inherited. In light of this result, we advocate further genetic, histological, and functional analyses to refine diagnosis and understand disease mechanisms.

DATA AVAILABILITY

All data generated or analyzed during this study are included in this published article and its supplementary files. The variants were submitted to Clinvar (Accession ID: SCV007106170, SCV007106171, SCV007106172, SCV007106173, SCV007106174).

REFERENCES

1. Jungbluth H, Sewry CA, Muntoni F. Core myopathies. Semin Pediatr Neurol. 2011;18:239–49. https://doi.org/10.1016/j.spen.2011.10.005.
2. Garibaldi M, Rendu J, Brocard J, Lacene E, Fauré J, Brochier G, et al. Dusty core disease' (DuCD): expanding morphological spectrum of RYR1 recessive myopathies. Acta Neuropathol Commun. 2019;7:3 https://doi.org/10.1186/s40478-018-0655-5.
3. Jungbluth H, Dowling JJ, Ferreiro A, Muntoni F. RYR1 Myopathy Consortium. 217th ENMC International Workshop: RYR1-related myopathies, Naarden. Neuromuscul Disord. 2016;26:624–33. https://doi.org/10.1016/j.nmd.2016.06.001.
4. Pelletier L, Petiot A, Brocard J, Giannesini B, Giovannini D, Sanchez C, et al. In vivo RyR1 reduction in muscle triggers a core-like myopathy. Acta Neuropathol Commun. 2020;8:192 https://doi.org/10.1186/s40478-020-01068-4.
5. Marty I, Robert M, Villaz M, De Jongh K, Lai Y, Catterall WA, et al. Biochemical evidence for a complex involving dihydropyridine receptor and ryanodine receptor in triad junctions of skeletal muscle. Proc Natl Acad Sci USA. 1994;91:2270–4. https://doi.org/10.1073/pnas.91.6.2270.
6. Zhou H, Rokach O, Feng L, Munteanu I, Mamchaoui K, Wilmshurst JM, et al. RyR1 deficiency in congenital myopathies disrupts excitation-contraction coupling. Hum Mutat. 2013;34:986–96. https://doi.org/10.1002/humu.22326.
7. Fusto A, Cassandrini D, Fiorillo C, Codemo V, Astrea G, D'Amico A, et al. Expanding the clinical-pathological and genetic spectrum of RYR1-related congenital myopathies with cores and minicores: an Italian population study. Acta Neuropathol Commun. 2022;10:54 https://doi.org/10.1186/s40478-022-01357-0.
8. Wu S. Central core disease is due to RYR1 mutations in more than 90% of patients. Brain. 2006;129:1470–80. https://doi.org/10.1093/brain/awl077.
9. Jungbluth H, Dowling JJ, Ferreiro A, Muntoni F. 182nd ENMC International Workshop: RYR1-related myopathies, 15-17th April 2011, Naarden, The Netherlands. Neuromuscul Disord. 2012;22:453–62. https://doi.org/10.1016/j.nmd.2011.12.003.
10. Dirksen R, Avila G. Altered ryanodine receptor function in central core disease: leaky or uncoupled Ca (2+) release channels? Trends Cardiovasc Med. 2002;12:189–97. https://doi.org/10.1016/s1050-1738(02)00163-9.
11. Jungbluth H, Treves S, Zorzato F, Sarkozy A, Ochala J, Sewry C, et al. Congenital myopathies: disorders of excitation-contraction coupling and muscle contraction. Nat Rev Neurol. 2018;14:151–67. https://doi.org/10.1038/nrneurol.2017.191.
12. Robinson R, Carpenter D, Shaw MA, Halsall J, Hopkins P. Mutations in RYR1 in malignant hyperthermia and central core disease. Hum Mutat. 2006;27:977–89. https://doi.org/10.1002/humu.20356.
13. Galli L, Orrico A, Lorenzini S, Censini S, Falciani M, Covacci A, et al. Frequency and localization of mutations in the 106 exons of the RYR1 gene in 50 individuals with malignant hyperthermia. Hum Mutat. 2006;27:830 https://doi.org/10.1002/humu.9442.
14. Jungbluth H, Zhou H, Hartley L, Halliger-Keller B, Messina S, Longman C, et al. Minicore myopathy with ophthalmoplegia caused by mutations in the ryanodine receptor type 1 gene. Neurology. 2005;65:1930–5. https://doi.org/10.1212/01.wnl.0000188870.37076.f2.

15. Natera-de Benito D, Ortez C, Jou C, Jimenez-Mallebrera C, Codina A, Carrera-García L, et al. The Phenotype and Genotype of Congenital Myopathies Based on a Large Pediatric Cohort. Pediatr Neurol. 2021;115:50–65. https://doi.org/10.1016/j.pediatrneurol.2020.11.002.
16. Davis MR, Haan E, Jungbluth H, Sewry C, North K, Muntoni F, et al. Principal mutation hotspot for central core disease and related myopathies in the C-terminal transmembrane region of the RYR1 gene. Neuromuscul Disord. 2003;13:151–7. https://doi.org/10.1016/s0960-8966(02)00218-3.
17. Zhou H, Jungbluth H, Sewry CA, Feng L, Bertini E, Bushby K, et al. Molecular mechanisms and phenotypic variation in RYR1-related congenital myopathies. Brain. 2007;130:2024–36. https://doi.org/10.1093/brain/awm096.
18. Chang X, Jin Y, Zhao H, Huang Q, Wang J, Yuan Y, et al. Clinical features and ryanodine receptor type 1 gene mutation analysis in a Chinese family with central core disease. J Child Neurol. 2013;28:384–8. https://doi.org/10.1177/0883073812441251.
19. Ogasawara M, Nishino I. A review of core myopathy: central core disease, multiminicore disease, dusty core disease, and core-rod myopathy. Neuromuscul Disord. 2021;31:968–77. https://doi.org/10.1016/j.nmd.2021.08.015.
20. Richards S, Aziz N, Bale S, Bick D, Das S, Gastier-Foster J, et al. Standards and guidelines for the interpretation of sequence variants: a joint consensus recommendation of the American College of Medical Genetics and Genomics and the Association for Molecular Pathology. Genet Med. 2015;17:405–24. https://doi.org/10.1038/gim.2015.30.
21. Bean LJH, Hegde MR. Clinical implications and considerations for evaluation of in silico algorithms for use with ACMG/AMP clinical variant interpretation guidelines. Genome Med. 2017;9:111. https://doi.org/10.1186/s13073-017-0508-z.
22. Gaspar BL. A novel homozygous variant of RYR1 p.Ala3072Asp in a neonate with dusty core disease: A new entity with clinicopathological implications. Neuropathology. 2020;40:367–72. https://doi.org/10.1111/neup.12648.
23. Vivekanandam V, Männikkö R, Matthews E, Hanna MG. Improving genetic diagnostics of skeletal muscle channelopathies. Expert Rev Mol Diagn. 2020;20:725–36. https://doi.org/10.1080/14737159.2020.1782195.
24. Schartner V, Romero NB, Donkervoort S, Treves S, Munot P, Pierson TM, et al. Dihydropyridine receptor (DHPR, CACNA1S) congenital myopathy. Acta Neuropathol. 2017;133:517–33. https://doi.org/10.1007/s00401-016-1656-8.
25. Nakai J, Sekiguchi N, Rando TA, Allen PD, Beam KG. Two regions of the ryanodine receptor involved in coupling with L-type Ca2+ channels. J Biol Chem. 1998;273:13403–6. https://doi.org/10.1074/jbc.273.22.13403.
26. Dulhunty AF, Haarmann CS, Green D, Laver DR, Board PG, Casarotto MG. Interactions between dihydropyridine receptors and ryanodine receptors in striated muscle. Prog Biophys Mol Biol. 2002;79:45–75. https://doi.org/10.1016/s0079-6107(02)00013-5.
27. Shishmarev D. Excitation-contraction coupling in skeletal muscle: recent progress and unanswered questions. Biophys Rev. 2020;12:143–53. https://doi.org/10.1007/s12551-020-00610-x.
28. Guis S, Figarella-Branger D, Monnier N, Bendahan D, Kozak-Ribbens G, Mattei JP, et al. Multiminicore disease in a family susceptible to malignant hyperthermia: histology, in vitro contracture tests, and genetic characterization. Arch Neurol. 2004;61:106 https://doi.org/10.1001/archneur.61.1.106.
29. Jeong SK, Kim DC, Cho YG, Sunwoo IN, Kim DS. A double mutation of the ryanodine receptor type 1 gene in a malignant hyperthermia family with multiminicore myopathy. J Clin Neurol. 2008;4:123 https://doi.org/10.3988/jcn.2008.4.3.123.
30. Herasse M, Parain K, Marty I, Monnier N, Kaindl AM, Leroy JP, et al. Abnormal distribution of calcium-handling proteins: a novel distinctive marker in core myopathies. J Neuropathol Exp Neurol. 2007;66:57–65. https://doi.org/10.1097/NEN.0b013e31802d47ce.
31. Dowling JJ, Lillis S, Amburgey K, Zhou H, Al-Sarraj S, Buk SJA, et al. King-Denborough syndrome with and without mutations in the skeletal muscle ryanodine receptor (RYR1) gene. Neuromuscul Disord. 2011;21:420–7. https://doi.org/10.1016/j.nmd.2011.03.006.
32. Snoeck M, van Engelen BGM, Küsters B, Lammens M, Meijer R, Molenaar JPF, et al. RYR1-related myopathies: a wide spectrum of phenotypes throughout life. Eur J Neurol. 2015;22:1094–112. https://doi.org/10.1111/ene.12713.

ACKNOWLEDGEMENTS

We thank the Associazione Centro Dino Ferrari for its support. Muscle biopsy and DNA samples were provided by the Bank of Muscle Tissue, Peripheral Nerve, DNA, and Cell Culture, member of Telethon Network of Genetic biobanks, at Fondazione IRCCS Ca' Granda, Ospedale Maggiore Policlinico, Milano, Italy. This work was promoted within the European Reference Network (ERN) for Neuromuscular Diseases. (M.S. as HCP Representative for the Italian ERN—NMD). The PNC "Hub Life Science-Diagnostica Avanzata (HLS-DA), PNC-E3-2022-23683266– CUP: C43C22001630001" is funded by the Italian Minister of Health. The support of Italian Ministry of Education and Research (MUR) "Dipartimenti di Eccellenza Program 2023–2027" - Dept of Pathophysiology and Transplantation, University of Milan to D.R. is gratefully acknowledged.

AUTHOR CONTRIBUTIONS

DP, SZ, interpreted the results; DP, SZ conceived the idea and revised the literature; DP, SZ wrote the manuscript; FM, MGD, EA, VN, MS performed clinical assessments; DP, SP, DR, DC, FFa performed genetic experiments; SS performed cells experiments; PC performed histological studies on muscle; SZ performed immunofluorescence experiments; MR and LN performed ultrastructural analysis; FFo performed Western Blot experiments; MS, SC, DR and GPC critically revised the final version of the manuscript. All the authors have read and approved the manuscript.

FUNDING

This study was funded by Italian Ministry of Health, Foundation IRCCS Ca' Granda Ospedale Maggiore Policlinico. Ricerca Corrente 2025 to GPC.

COMPETING INTERESTS

The authors declare no competing interests.

ETHICS APPROVAL

The study was conducted in accordance with the Declaration of Helsinki and approved by the local Ethics Committee RebiNeu 186771, "IRCCS Ca' Granda Foundation Ospedale Maggiore Policlinico, Milan, Italy".

CONSENT FOR PUBLICATION

Informed consent was obtained from all subjects involved in the study.

ADDITIONAL INFORMATION

Supplementary information The online version contains supplementary material available at https://doi.org/10.1038/s41431-026-02080-3.

Correspondence and requests for materials should be addressed to Daniela Piga.

Reprints and permission information is available at http://www.nature.com/reprints

Publisher's note Springer Nature remains neutral with regard to jurisdictional claims in published maps and institutional affiliations.